

Circular array transducer based-photoacoustic/ultrasonic endoscopic imaging with tunable ring-beam excitation

Zhihua Xie^{a,b,1}, Jiamei Liu^{b,c,1}, Yaguang Ren^{a,b,1}, Jiqing Huang^{b,c}, Riqiang Lin^{a,b},
 Xi Tian Wang^{a,b}, Qingyuan Tan^{b,c}, Shengmiao Lv^{a,b}, Liang Song^{a,b}, Chengbo Liu^{a,b,*},
 Teng Ma^{b,c,**}, Xiaojing Gong^{a,b,*}

^a Research Laboratory for Biomedical Optics and Molecular Imaging, Guangdong Provincial Key Laboratory of Biomedical Optical Imaging Technology, Shenzhen Institutes of Advanced Technology, Chinese Academy of Sciences, Shenzhen 518055, China

^b CAS Key Laboratory of Health Informatics, Shenzhen Institutes of Advanced Technology, Chinese Academy of Sciences, Shenzhen 518055, China

^c Paul C. Lauterbur Research Center for Biomedical Imaging, Shenzhen Institutes of Advanced Technology, Chinese Academy of Sciences, Shenzhen 518055, China

ARTICLE INFO

Keywords:

Photoacoustic/ultrasonic endoscopy
 Tunable ring-beam
 Circular array transducer
 Imaging distance
 Optical excitation efficiency
 PAE/EUS probe

ABSTRACT

Photoacoustic/ultrasound endoscopic imaging is regarded as an effective method to achieve accurate detection of intestinal disease by offering both the functional and structural information, simultaneously. Compared to the conventional endoscopy with single transducer and laser spot for signal detection and optical excitation, photoacoustic/ultrasound endoscopic probe using circular array transducer and ring-shaped laser beam avoids the instability brought by the mechanical scanning point-to-point, offering the dual-modality imaging with high accuracy and efficiency. Meanwhile, considering the complex morphological environments of intestinal tracts in clinics, developing the probe having sufficient wide imaging distance range is especially important. In this work, we develop a compact circular photoacoustic/ultrasonic endoscopic probe, using the group of fiber, lens and home-made axicon, to generate relatively concentrated ring-shaped laser beam for 360° excitation with high efficiency. Furthermore, the laser ring size can be tuned conveniently by changing the fiber-lens distance to ensure the potential applicability of the probe in various and complex morphological environments of intestines. Phantom experimental results demonstrate imaging distance range wide enough to cover from 12 mm to 30 mm. In addition, the accessibility of the photoacoustic signals of molecular probes in ex vivo experiments at the tissue depth of 7 mm using excitation energy of 5 mJ has also been demonstrated, showing a high optical excitation efficiency of the probe.

1. Introduction

Intestinal diseases have become increasing problem in the world. For example, colorectal cancer is responsible for 935173 deaths worldwide in 2020, ranking the second place of cancer deaths [1]; inflammatory bowel disease generally involves abdominal pain, diarrhea, bloody stools, weight loss, leading to lifelong pain to the patients [2,3]. These diseases bring severe economic and social burden to the world. Diagnosing the disease accurately holds great importance. In clinics, endoscopic imaging technologies have become the main tool for accurate

diagnosis of intestinal disease by offering the morphological or functional information of the disease lesions with high imaging resolution and sensitivity.

During the past decades, optical endoscopies, such as white-light endoscopy [4], narrow-band imaging [5], optical fluorescence imaging [6,7], optical coherence tomography [8,9], took important place in intestinal disease diagnosis by imaging the diseased tissues with high sensitivity and high spatial resolution. However, the application of these technologies is limited either by lack of depth resolution or superficial imaging depth. Endoscopic ultrasound (EUS) is an imaging modality

* Corresponding authors at: Research Laboratory for Biomedical Optics and Molecular Imaging, Guangdong Provincial Key Laboratory of Biomedical Optical Imaging Technology, Shenzhen Institutes of Advanced Technology, Chinese Academy of Sciences, Shenzhen 518055, China.

** Corresponding author at: CAS Key Laboratory of Health Informatics, Shenzhen Institutes of Advanced Technology, Chinese Academy of Sciences, Shenzhen 518055, China.

E-mail addresses: cb.liu@siat.ac.cn (C. Liu), teng.ma@siat.ac.cn (T. Ma), xj.gong@siat.ac.cn (X. Gong).

¹ Zhihua Xie, Jiamei Liu and Yaguang Ren contribute equally to this work

which can provide detailed structural information about intestinal wall and adjacent organs [10–12]. It is highly accurate in the visualization of submucosal lesions and their sonographic layer of origin within the intestinal wall, thus EUS has become a commonly-used diagnosis method in clinics. Besides the structural information, functional information is also essential in intestinal disease diagnosis, which is beyond the detection ability of EUS.

Photoacoustic endoscopy (PAE) has attracted more and more attention given its capability of functional information detection, especially for the diseased tissues in deep. Photoacoustic imaging is based on light absorption and ultrasound signal detection, acquiring volumetric and functional information of the tissues [13–15]. The basic principle determines the technology high imaging contrast and large imaging depth [14]. Several studies have demonstrated the acquisition of the characteristics of endothelial tissue using both ultrasound and photoacoustic imaging [16–18]. Furthermore, photoacoustic and ultrasonic integrated endoscopies (PAE/EUS) have also been proposed to acquire both the structural and functional information in intestinal diseases. Wang's group intervened a single ultrasonic transducer-based PAE/EUS into esophagus of rabbits, acquiring the photoacoustic and ultrasonic images of surrounding tissues and proximal organs in vivo [19]. Then several PAE/EUS systems with full field-of-view have been proposed by Chen's group, Song's group, Xing's group and Zhu's group, to visualize the vasculature on colorectal wall in vivo [20–24]. Recently, Ntziachristos's group proposed a capsule endoscopy with outer diameter of 16 mm and imaging speed of video rate of 50 Hz [25]. Although the above-mentioned studies demonstrated the capability of PAE/EUS in acquiring accurate functional and structural information, the hybrid optical and electrical rotary joints in the systems generally brings unexpected issues during high-speed scanning, such as the damage of optical joints by pulsed laser, electrical noise, non-uniform rotation, etc [20]. The endoscopy composed of circular transducer array is an alternative to offer cross-sectional image by each pulse excitation, with no need of point-by-point scanning. Xing's group proposed a single-modality PAE system based on a circular transducer array and ring-shaped laser excitation, differentiating between colorectal cancer and normal colorectal tissues *ex vivo* by evaluating photoacoustic signals [26]. But the clinical transition of the probe is quite difficult since the imaging distance range was not demonstrated and the single PAE modality is difficult to be applied in intestinal environment in vivo without the guidance of ultrasound imaging. In addition, compared to the size of the clinical endoscopies of around 10 mm, the probe diameter of 30 mm will bring more difficulties in clinical applications. To push the PAE/EUS probe with circular excitation and detection forward to clinics, it is necessary to develop the probe with the imaging distance range wide enough to cover various intestinal tracts in clinics under the premise of limited probe size.

In this research, we develop a circular transducer array-based PAE/EUS probe with tunable ring-shaped laser beam for 360° optical excitation based on fiber and relevant optical elements. The optical excitation efficiency is assured that the photoacoustic signal of the molecular probes at the tissue depth of 7 mm can be captured using the excitation energy of 5 mJ. The diameter of the ring-shaped laser beam can be tuned conveniently by moving fiber axially, with the resultant photoacoustic imaging distance range covering from 12 mm to 30 mm. The wide imaging distance range makes the probe especially suitable for the application in complex intestinal environments. In addition, the outer diameter of 11 mm of the probe makes it a potential candidate in clinical endoscopic applications.

2. Materials and methods

2.1. Principle of light ring generation and tunability

The fiber, lens and axicon are used to generate the ring-shaped laser beam. The laser beam output from the fiber is reshaped by a lens, then

passes through an axicon to form the laser ring. When the fiber-lens distance is changed, the diameter of the ring-shaped beam is tuned correspondingly. To demonstrate the principle of light ring generation and tunability, we designed the experimental scheme in [Supplementary Fig. S1](#); and then the simulation and experimental results are obtained as shown in [Supplementary Fig. S2](#). When applied with the circular array ultrasonic transducer, a mirror is used in front of axicon to reflect the ring-shaped beam to the detection area of the ultrasonic probe. The optical/ultrasonic overlap area is compatible with the intestinal tract with different calibre, potentially acquiring the important information in different environments. The principle of the PAE/EUS probe and the distance tuning for photoacoustic imaging can be found in [Fig. 1\(a\)](#) and [\(b\)](#). When the fiber output end is positioned at P1 (small fiber-lens distance), a small ring-shaped beam is formed at the ultrasonic field; when positioned at P2 (large fiber-lens distance), a large ring-shaped beam is formed at the ultrasonic field.

2.2. PAE/EUS catheter design

The PAE/EUS catheter designed in this study consists of optical beam delivery system and a circular-array ultrasonic probe. The ultrasonic array consists of 192 transducer elements (element length: 5.825 mm, width: 0.1306 mm) at the central frequency of 7.5 MHz and distributed circularly around the probe. Each array element consists of one rows of piezoelectric pillars, so each element can be viewed as flat [24]. The picture of the transducer array is shown in [Fig.S3](#). The probe was used for 360° ultrasonic/photoacoustic imaging. A hollow channel (4 mm diameter) at center was drilled through the probe axially, offering the space for optical fiber (600 μm core diameter and 0.22 NA) to deliver light. A lens (9 mm focal length, 9 mm diameter) and a home-made axicon (conical angle of 84.5°, 9 mm diameter) were placed in front of the ultrasonic probe to generate the light ring. The fiber can be moved axially to change the fiber-lens distance, and furthermore, to tune the ring diameter. The lens and axicon were placed axially inside a 3D-printed tube, which is sealed closely on the end of the ultrasonic probe to protect the optical elements from the outer environment. A home-made convex mirror (radius of curvature: 100 mm, diameter: 9 mm) was used to reflect the light ring to the ultrasonic detection area for 360° photoacoustic excitation. The mirror was finally supported by transparent silicon tube which was attached to the end of 3D-printed tube. The PAE/EUS probe was generally applied downside in water and two holes were drilled on the wall of the silicon tube to fill water inside. The principle of PAE/EUS probe are shown in [Fig. 1\(c\)](#), [\(d\)](#), respectively.

2.3. Photoacoustic and ultrasonic imaging system

The block diagram of the imaging system is shown in [Supplementary Fig. S4](#). It consists of a nano-pulsed OPO laser source (Innolas 100 Hz), optical lens, a Vantage 256 research ultrasound platform (Verasonics Inc., Kirkland, WA, USA), a computer and the proposed PAE/EUS probe. In the research, the laser at the wavelength of 780 nm and laser energy of 5 mJ is used for photoacoustic excitation. During the imaging, the ultrasound elements emit and receive the ultrasonic signals to form ultrasound image at the repetition frequency of 100 Hz; then an external signal of 100 Hz is used to trigger data acquisition card of the Verasonic system to detect the ultrasonic signals; after a delay time of 250 μs, a signal is sent to laser by the Verasonics and trigger laser pulse generation; finally, the Verasonic system detects photoacoustic signal and form photoacoustic image.

2.4. Phantoms preparation and imaging

To evaluate the imaging resolution and distance, a 3D-printed phantoms were made with a hole at the center. Six tungsten wires (80 μm) were fixed at different distances around the hole. The distances

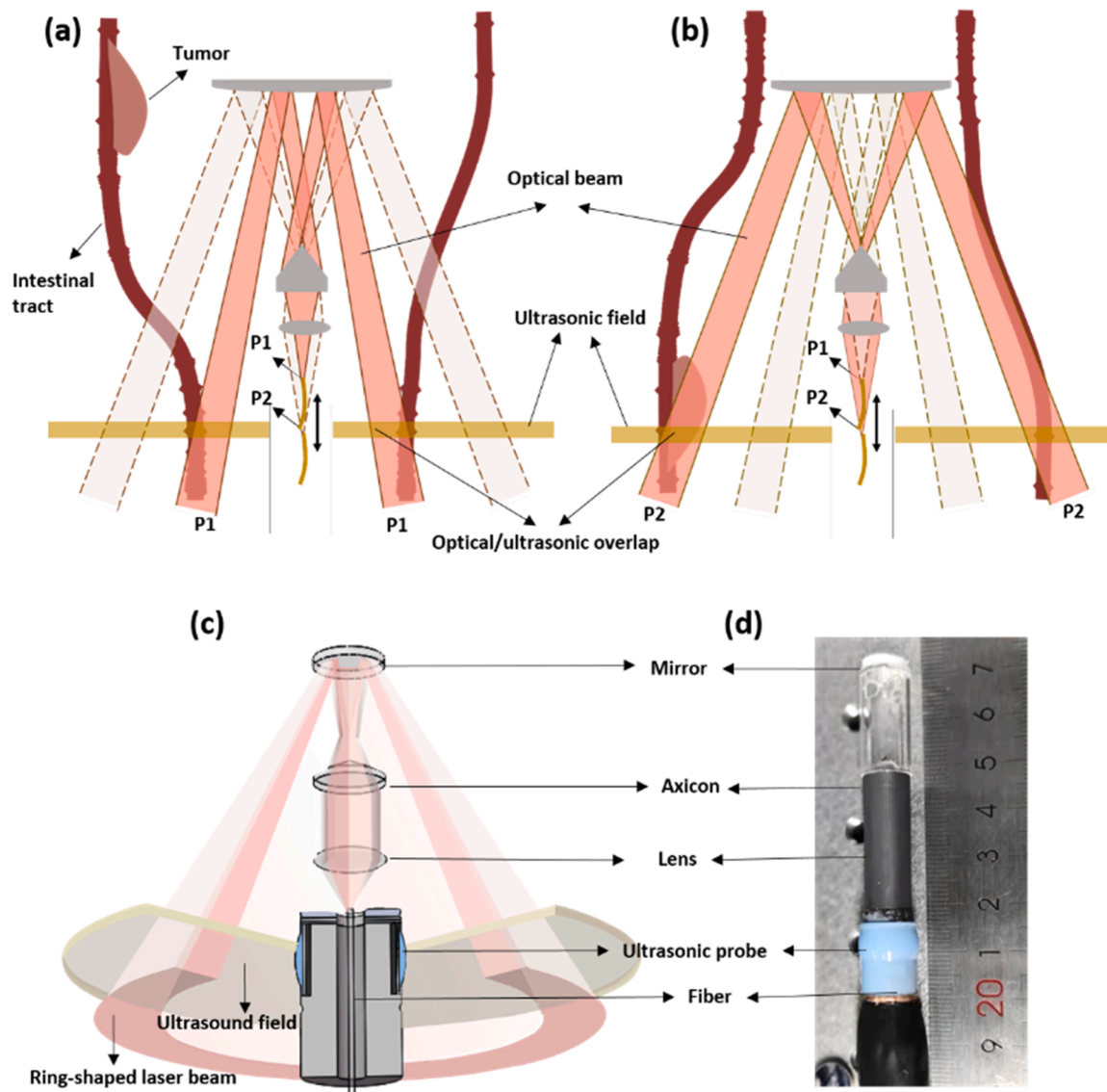


Fig. 1. (a), (b) The scheme of ultrasound field and optical beam overlapped at different distance with fiber position at P1 (a) and P2 (b), respectively, which are adaptable for the intestinal tracts with different size; (c) The PAE/EUS probe structure and optical/ultrasonic field distribution; (d) The picture of PAE/EUS probe.

of the six tungsten wires are 12 mm, 16 mm, 20 mm, 24 mm, 30 mm and 32 mm, respectively. During the imaging experiment, the whole phantom was fixed in water and the PAE/EUS probe was placed inside the hole axially. The optical fiber was moved axially to excite the tungsten wires at different distances.

To demonstrate the 360° imaging ability of the system, we used 3D-printed stent as the target. The diameter of the stent is 3 cm.

2.5. Ex vivo experiments

During the *ex vivo* experiment, we prepared three pig rectums. The mixture of ICG and agar at the concentration of around 1 mg/mL was prepared to offer photoacoustic signals in the experiments. For the first rectum, a vessel on the rectum wall was flushed by saline and filled with the mixture of ICG and agar. At the inner wall of the rectum, we injected the mixture of ICG and agar in situ. The second and the third pig rectums have different calibre (around 2.5 cm inner calibre and 3.6 cm inner calibre, respectively). The mixture of ICG and agar was injected both into the inner wall and the outer wall of the two rectums in situ. All the rectums were finally fixed inside agar gels and the gel inside the rectums was removed, leaving the hollow space for the imaging probe.

During the imaging experiment of the first rectum, the optical fiber was fixed where the maximum photoacoustic signals are generated from the ICG on the rectum. A pull-back motorized translation stage was used to move the probe to scan the rectum and form the 3D photoacoustic and ultrasonic images.

In the imaging experiment of the second and third rectum, the imaging probe was located at the position of the ICG. The optical fiber was moved axially to excite the ICG at different depth of the rectum wall and acquire the photoacoustic signals of the ICG targets.

2.6. Data process

For the quantification of signal-noise-ratio (SNR) of photoacoustic image, we firstly choose the region of interest (ROI) where the photoacoustic signal of the target locates and quantify the photoacoustic signals, then choose an area with no photoacoustic signal source and quantify the standard deviation (STD) of this area. The SNR in this study is finally quantified according to the following formula:

$$SNR = 20 * \log \frac{Signal_{PA}}{STD} \quad (1)$$

For the quantification of the lateral resolution from tungsten wire experiments, we obtained the photoacoustic/ultrasonic signal distribution along the lateral direction of the wire signal. The half-height peak width of the signal distribution curve offers the lateral resolution of the probe. The imaging resolution at four different distances were quantified finally.

2.7. Optical simulation

The optical simulation of the system was performed using the software of ZEMAX. The optical elements, including optical fiber, lens, axicon and mirror were modeled in the software and recorded the ring-shaped distribution of the beam at the signal detection area of the ultrasonic probe.

2.8. The reconstruction of photoacoustic and ultrasonic imaging

The Vantage system was used to drive the circular array transducer and save radio frequency (RF) signals, including ultrasonic signal and photoacoustic signal. The photoacoustic and ultrasound images are reconstructed by beamforming the RF signals using delay-and-sum method. During the reconstruction, ultrasonic signal was log compressed to produce the final ultrasonic image; the photoacoustic signal was used directly to produce the final photoacoustic image.

3. Results

Fig. 2 shows the simulation results of the light ring generated at the detection area of the ultrasonic probe. When the fiber-lens distance (d in Fig. 2) is fixed at 6 mm, 8 mm, 10 mm and 12 mm, the light rings are shown in Fig. 2(a)-(d), respectively. The maximum intensity of the rings

locates at 16 mm, 20 mm, 23.2 mm and 25.6 mm, respectively. It is obvious that the light ring gets bigger with the fiber-lens distance becoming larger. The cross-sectional light energy distribution of the rings in (a)-(d) in one direction is shown in (e). If we take the $1/e$ of the maximum light intensity of the ring in (d) as the threshold, the overall light ring after changing the fiber-lens distance is distributed on the area at radial radius of around 12–30 mm, as shown in (f). Based on the simulation results, we expect an accessibility of the photoacoustic signal information at the distance as large as 30 mm.

Fig. 3 shows the imaging results of tungsten wire phantom. We controlled the fiber-lens distance at 6 mm and 10 mm, then the photoacoustic images of the phantom are shown in Fig. 3(a) and (b), respectively. In Fig. 3(a), the signal of first three tungsten wires is clearly visible. In Fig. 3(b), we can see the photoacoustic signal of the third and the fourth tungsten wires is obvious, while the signal of the first two wires disappeared. It is notable that the signal of the fifth wire was also captured, but almost invisible due to the poor signal. The signal of the sixth wires was not captured. By choosing the optimal signal at every distance during scanning, we obtained the final photoacoustic imaging of the phantom as shown in Fig. 3(c), that is the signal of the first two wires from Fig. 3(a), while the signal of the third and the fourth wire from Fig. 3(b). The quantified SNR of the five wires are 19.8 dB, 38 dB, 33 dB, 19.6 dB and 12 dB, respectively. As a reference, we show the tungsten phantom picture in Fig. 3(d).

The lateral resolution curves we extract from the photoacoustic and ultrasonic images of tungsten wires in Fig. 3(c) are shown in Fig. 4. The photoacoustic and ultrasonic imaging resolution are measured three times at each distance. The averaged lateral resolution of photoacoustic images of 544 μm , 996 μm , 1160 μm and 1283 μm at the first four distances in Fig. 3(c) are shown in Fig. 4(a). Correspondingly, the averaged lateral resolution of ultrasonic image is 410 μm , 785 μm , 960 μm ,

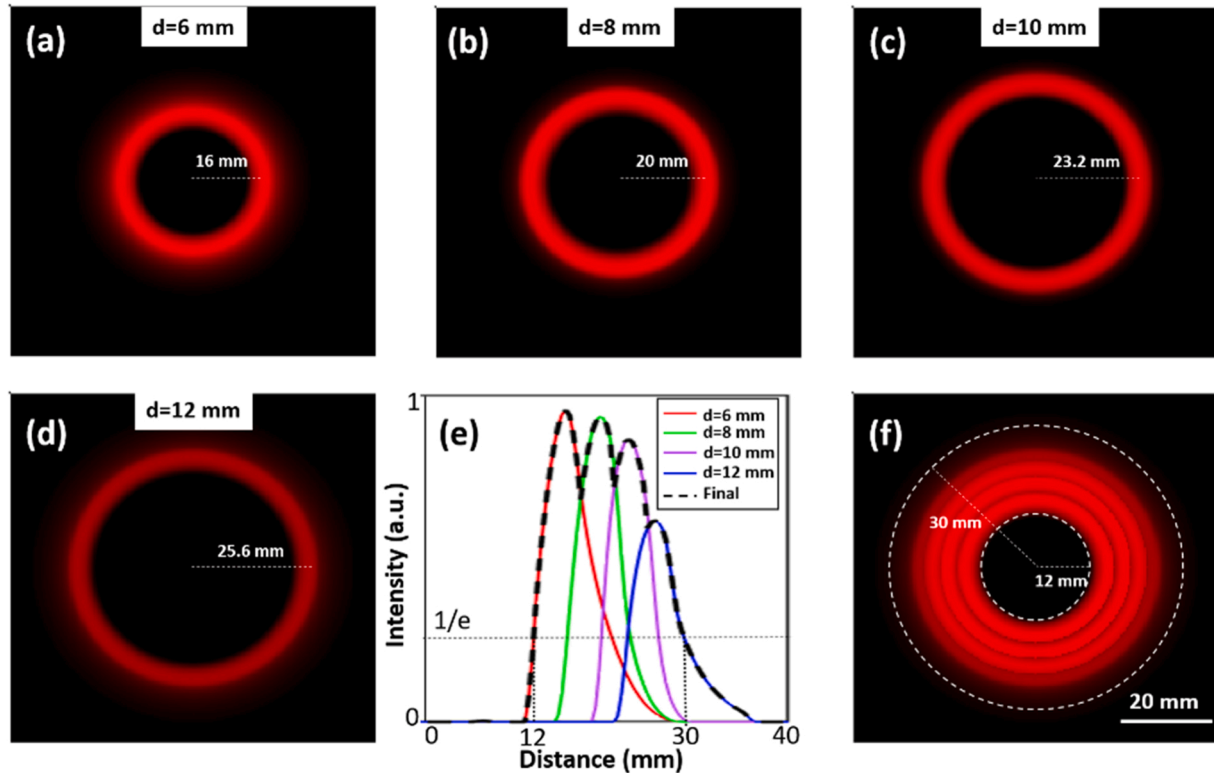


Fig. 2. The simulation results of the light ring formed at the detection area of the ultrasonic probe, with the fiber-lens distance of (a) $d=6$ mm, (b) $d=8$ mm, (c) $d=10$ mm and (d) $d=12$ mm. The values shown in the figures are the radius of the light rings where the maximum intensity locate. (e) The cross-sectional light energy distribution of the light ring in one direction is (red), (b) (green), (c) purple and (d) (blue). The final light distribution is described by the black dashed line. The light intensity at the black dashed line is $1/e$ of the maximum intensity of the light ring in (d). (f) The final light distribution of the rings after distance tuning. The white dashed circles are 12 mm and 30 mm radius, respectively. The two circles are where the light fluence is $1/e$ of the maximum intensity in (d).

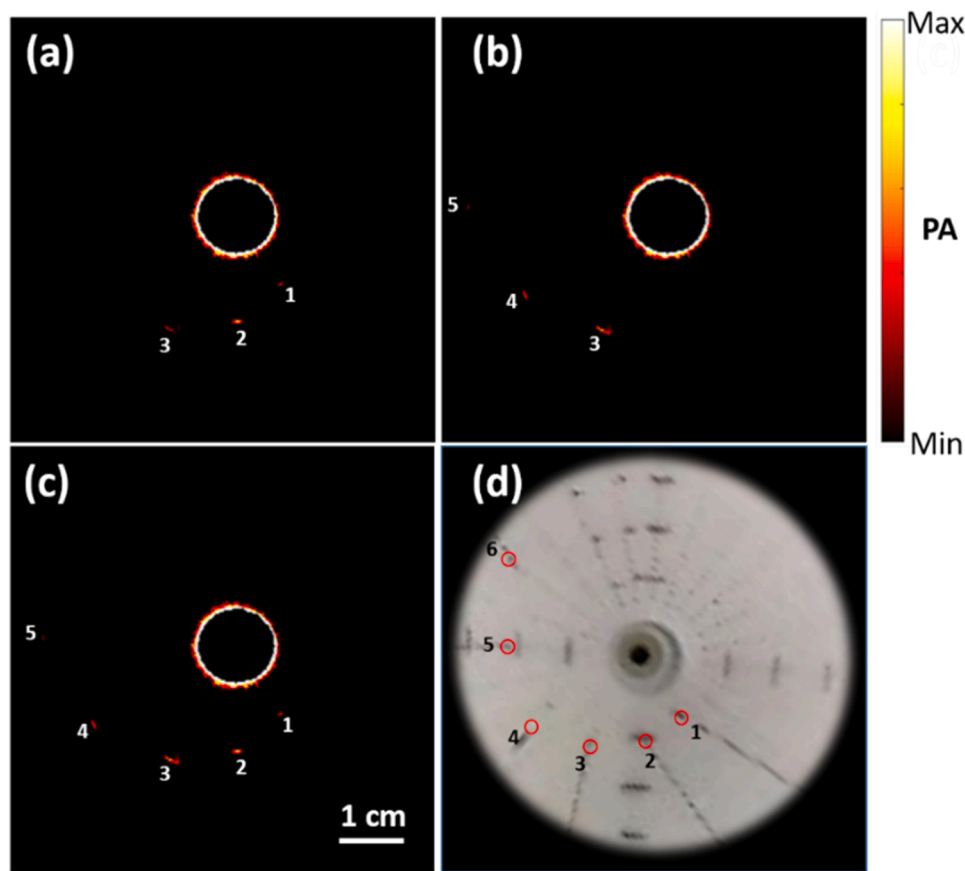


Fig. 3. Imaging results of tungsten wires at six different distances. The photoacoustic images of the phantom at the fiber-lens distance of 6 mm (a) and 10 mm (b), respectively. (c) The photoacoustic image of the phantom after distance tuning. (d) The picture of tungsten wire phantom.

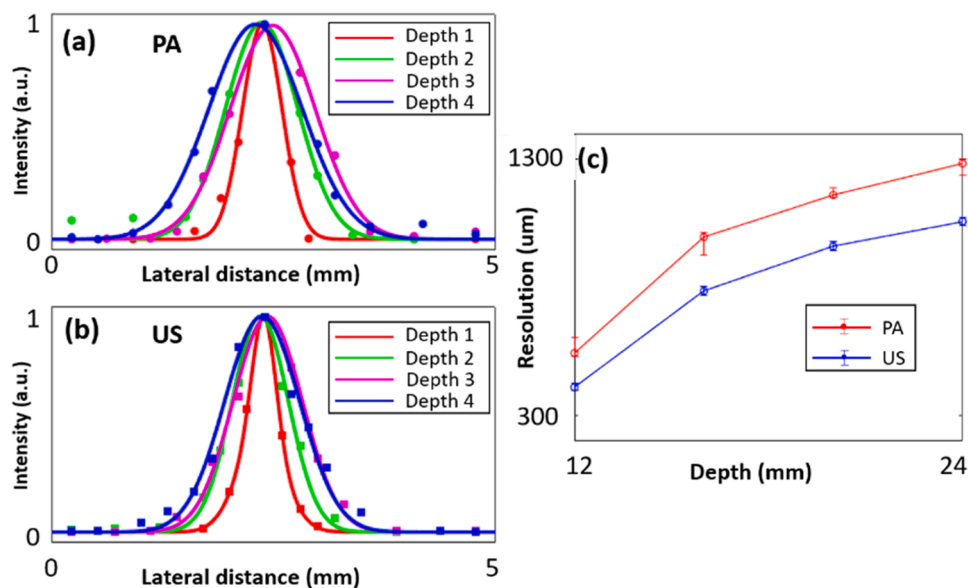


Fig. 4. The lateral signal intensity distribution of the tungsten wires at four different distances of (a) photoacoustic image and (b) ultrasonic image, respectively. (c) The lateral resolution of photoacoustic image (red) and ultrasonic image (blue) at different distances.

1057 μm, respectively, as shown in Fig. 4(b). The lateral resolution of the ultrasonic image is consistent with previous studies of the circular ultrasound probe with similar parameters [24]. The lateral resolution of photoacoustic image (red) and ultrasonic image (blue) at different distances are summarized in Fig. 4(c).

To demonstrate the 360° imaging ability of the system, we imaged a stent with the diameter of 30 mm, as shown in Fig. 5(a). The photoacoustic and ultrasonic imaging results of the stent are shown in (b)-(d) and (e)-(g), respectively. The results show continuous photoacoustic signal around 360°. The maximum SNR and minimum SNR of the

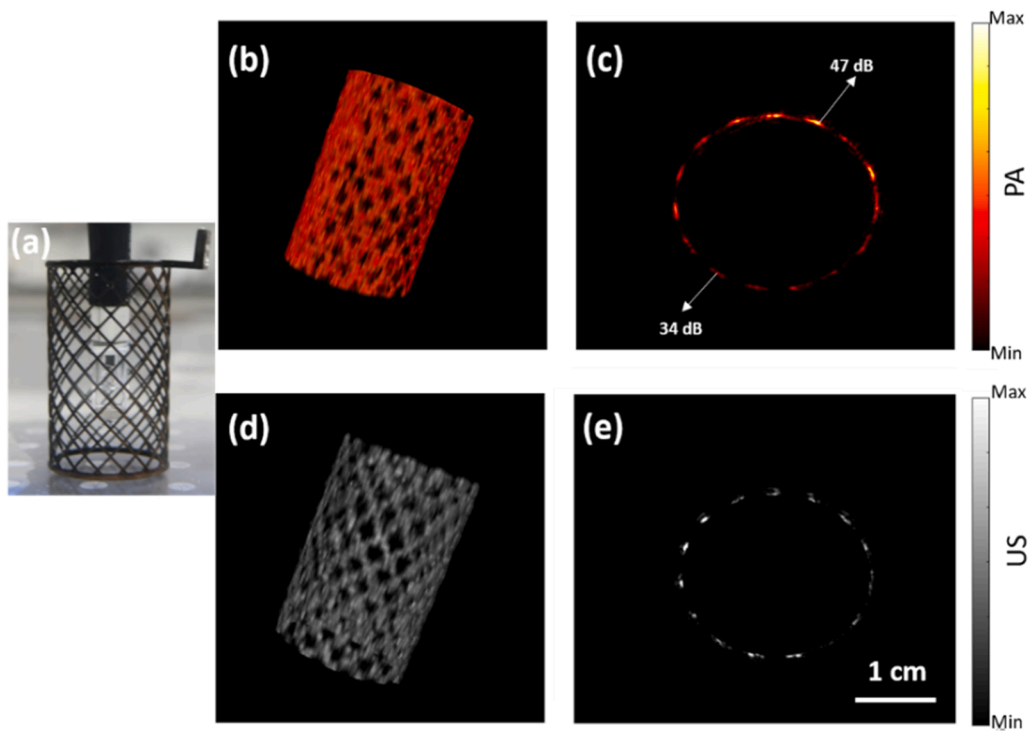


Fig. 5. (a) The picture of the stent with diameter of 30 mm. 3D reconstructed Photoacoustic (b) and Ultrasonic (d) image of the stent. (c) The cross-sectional photoacoustic image of the stent. (e) The cross-sectional ultrasonic image of the stent at the corresponding axial position of (c).

photoacoustic image around 360° are 68 dB and 52 dB, respectively. It is mainly due to the non-homogeneous distribution of the ring-shaped laser beam around 360°.

The 3D photoacoustic/ultrasonic imaging results of the pig rectum is shown in Fig. 6. Using the ex vivo pig rectum as shown in Fig. 6(a), we obtained the fused 3D photoacoustic/ultrasonic image as shown in Fig. 6(b). The ultrasonic image showing the structure of the rectum wall and

the photoacoustic image showing the ICG information on the wall were captured simultaneously. The photoacoustic signals were shown in Fig. 6(c), with the signals from ICG in vessels and on inner wall clearly seen. The B-scan fused image and photoacoustic image in one cross-section is shown in Fig. 6(d) and Fig. 6(e), respectively.

The photoacoustic and ultrasonic imaging results of the ex vivo pig intestines are shown in Fig. 7. Fig. 7(a)-(c) shows the imaging results of

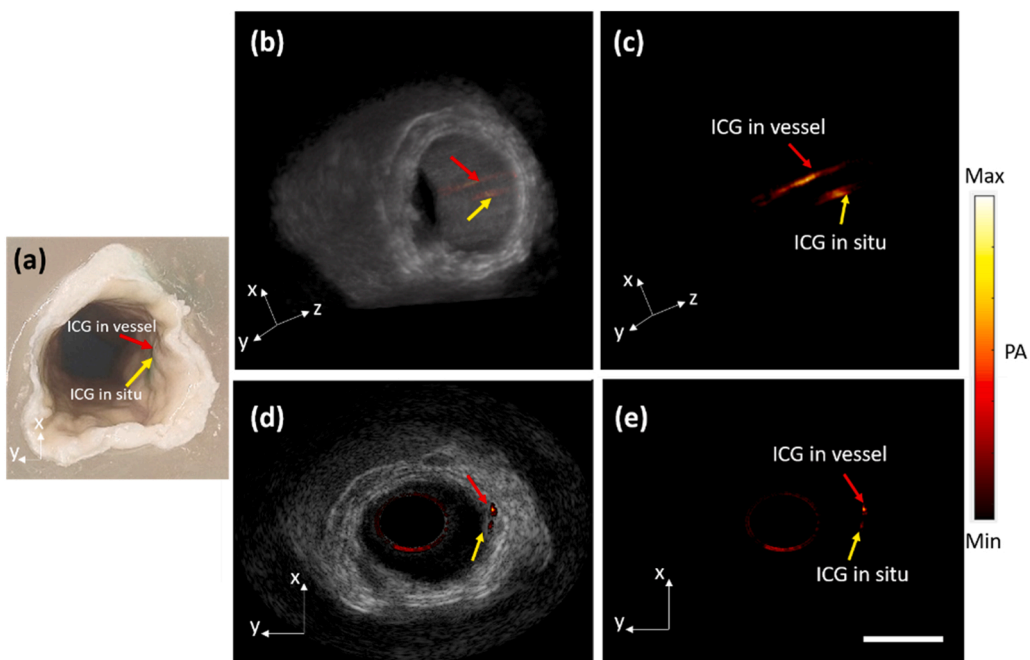


Fig. 6. (a) The picture of an ex vivo pig intestine. The red arrow and the yellow arrow indicate the orientation of vessel and ICG in situ, respectively. (b) 3D fused Photoacoustic/Ultrasonic image of ex vivo intestine as shown in (a); (c) 3D Photoacoustic image of ex vivo intestine as shown in (a); (d) Photoacoustic/Ultrasonic fused B-scan image of a cross-section in (b); (e) Photoacoustic B-scan image of a section in (c). scale bar : 1 cm.

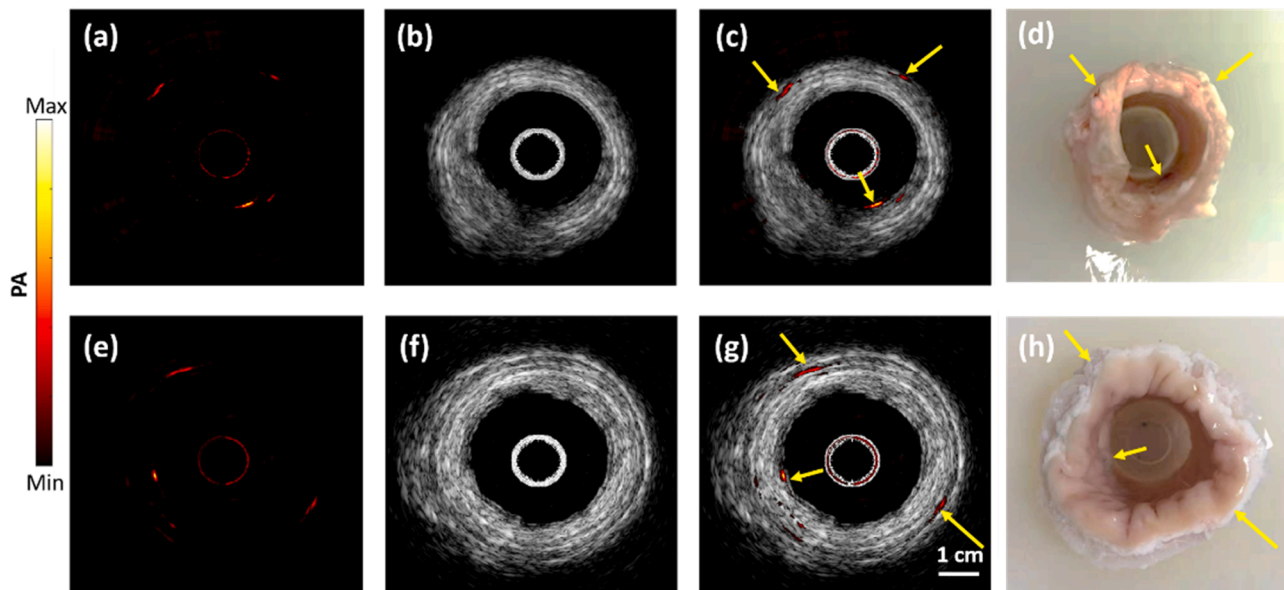


Fig. 7. (a) Photoacoustic, (b) Ultrasonic and (c) Photoacoustic/Ultrasonic image of an ex vivo intestine as shown in (d); (e) Photoacoustic, (f) Ultrasonic and (g) Photoacoustic/Ultrasonic image of an ex vivo intestine as shown in (h). The yellow arrows in (d) and (h) show the location of ICG.

an intestine with the inner calibre of 25 mm and outer calibre of 46 mm (Fig. 7(d)). The functional information (ICG) from both the inner and outer wall of the intestine can be clearly found, while structural information of the intestine is offered in the ultrasonic images. Similar imaging results are obtained in an intestine with larger calibre (Fig. 7(h): inner calibre of 36 mm and outer calibre of 50 mm), as shown in (e)-(g). The intestinal calibre was quantified from the ultrasound image. From the experimental results we can see, although the excitation laser suffers scattering by the intestinal wall of the thickness of around 7 mm, the photoacoustic signal on the outer wall of the intestine can also be captured successfully. It demonstrates the capability of the probe in detecting the photoacoustic signal in deep using the excitation energy of 5 mJ.

4. Discussion

PAE/EUS is an important tool in the early diagnosis of intestinal diseases. Compared to the probes with single ultrasound transducer for signal detection and point-to-point scanning for final imaging, the PAE/EUS probes using circular transducer array and ring-shaped laser beam hold the advantages in accurate and efficient imaging. In previous clinical studies, we knew that the calibre of human adults' intestinal tracts distributed within a wide range [28], and some disease, such as tumors, also lead to the morphological change of intestinal cavity. Thus, the clinical intestinal environments are always complex. Developing endoscopic probe which is widely suitable for the complex cavity environments is clinically significant. The most important prerequisite of the suitability is that the imaging distance range of the probe is sufficient wide to cover the intestinal wall in different environments. In this study, we proposed a circular transducer array-based PAE/EUS probe using tunable ring-shaped beam for photoacoustic excitation. The final photoacoustic imaging distance range is wide enough to cover most intestinal walls. In addition, the probe diameter of 11 mm is sufficient small for smoothly passing through the intestinal tract.

We firstly focused on the wide imaging distance range of the probe in this study. It is obvious that photoacoustic imaging distance range is mainly decided by the distribution of the ring-shaped laser beam. The broad distribution of the beam covering large area generates the photoacoustic imaging with wide imaging distance range, but lowers the optical fluence and further, leads to a moderate excitation efficiency. In

this study, we used a group of optical elements, including fiber, lens and axicon, to generate the ring-shaped laser beam in a relatively concentrated way, which is important in improving photoacoustic excitation efficiency; then tuned the ring diameter flexibly by changing the fiber-lens distance to keep wide imaging distance range, with the final imaging distance range covering from 12 m to 30 mm. Thus, good excitation efficiency and wide imaging distance range were achieved simultaneously in this study. The experimental results of tungsten wire phantom in Fig. 3 demonstrated the accessibility of the photoacoustic signal from the distance of 12–30 mm. At the distance of 32 mm, the photoacoustic signal of the wire was not captured.

Moreover, the optical excitation efficiency is also ensured using this probe. It is noticeable that the optical fluence is quite difficult to quantify accurately due to the changed ring-shaped beam distribution at different distances, the uncertainty of the decentration of the optical elements in reality. But by optical simulation, we can obtain the optical distribution with and without decentration of the optical elements, as shown in Fig.S5. Furthermore, the maximum optical fluence can be deduced roughly using the total excitation energy and the theoretical light distribution. In this study, we used the excitation energy of 5 mJ, the maximum optical fluence was deduced less than 1 mJ/cm^2 , much lower than ANSI threshold: 20 mJ/cm^2 . In the ex vivo experiments, the molecular probes of ICG both from the inner wall and outer wall of the ex vivo pig intestines were successfully identified. Considering the intestinal wall thickness of around 7 mm, the photoacoustic imaging of the probe shows a good excitation efficiency and great superiority in accessibility of the target in deep of the tissues.

To assure the PAE/EUS probe passing the intestines smoothly, the diameter of the probe should be kept as small as possible. The diameter of the probe developed in this study is 11 mm, which is comparable with the size of clinical endoscopies and potential for intervening most of the human intestines. The small size of the PAE/EUS probe is attributed to the small size of the ultrasonic probe on one side; on the other side, we made full use of the hollow channel in the ultrasonic probe and the outer space in front of the probe to integrate the optical elements for the laser ring generation and tunability. The optical elements were designed elaborately to keep the outer diameter of the probe unchanged. Although the rigid length of the probe was increased, the outer diameter was successfully kept at 11 mm, which provides the basis for the practical application in the future.

The resolution results (Fig. 4) demonstrated the ability of our system in identifying disease lesions. In this study, we obtained the lateral resolution of ultrasonic image consistent with previous studies of the circular ultrasound probe with similar parameters [27]. The lateral resolution of photoacoustic image is demonstrated a little worse than ultrasonic image. As we all know, the lateral resolution of ultrasonic image is theoretically decided by the convolution of the ultrasonic emission and detection, while the lateral resolution of photoacoustic image is decided by the signal detection. In this case, photoacoustic imaging generally shows a lower lateral resolution than ultrasonic imaging. In addition, the lateral resolution of around 500 μm is sufficient to identify the disease lesion as small as 1 mm [29], which is generally very early stage in the intestinal tumor development [30].

Although we demonstrated the feasibility of the PAE/EUS probe in 360° photoacoustic and ultrasonic imaging, there are still some works we can continue in the future. For example, in the frame of current probe design, we kept the diameter of the probe as small as possible. However, as we mentioned before, the final rigid length of the optical part of the probe is as long as 5 cm, which restricts the potential in vivo applications to very limited endoscopic circumstances. In the future, it is possible to shorten the probe by leaving space at the side wall of the probe for light passing, then forming the ring-shaped beam inside the hollow channel of the probe, thus we can make full use of the hollow channel inside the probe and save the space out of the probe. Secondly, the ring-shaped laser beam generation was mainly due to the light refraction at the tiny cone of axicon, which raised strict requirement of optical alignment. Subtle decentration of optical elements (optical fiber, lens, axicon) lead to obvious non-uniform distribution of the light ring around 360°, as shown in Fig.S4. The imaging results of stents demonstrated that the energy distribution of the laser was continuous around 360°, but the uniformity of the ring-shaped laser beam around 360° is not good, resulting in the maximum and minimum SNR of 68 dB and 52 dB, respectively. In the future, optimizing the centering of the optical elements and improving the centration of optical path are necessary to uniform the laser distribution. In addition, the in vivo experiments should be performed to demonstrate the practicality of the probe in alive animals.

5. Conclusion

In this study, we developed a compact PAE/EUS probe, offering 360° functional and structural information of targets. The outer diameter of 11 mm makes it suitable for most clinical intestines intervening. The lateral resolution of 544 μm demonstrates the ability of the probe in detecting the miniature disease lesions. By tuning the fiber conveniently, the photoacoustic imaging distance was expanded to 12–30 mm, quite compatible with the complex intestine environments in clinics. The imaging results of pig intestines with larger and smaller calibre demonstrated the flexibility of the probe application in different environments. Meanwhile, the successful photoacoustic imaging of ICG at the inner and outer wall of pig intestine showed the accessibility of the functional information both at the inner surface and in deep using the probe. In sum, we proposed a PAE/EUS probe having the imaging distance range compatible with clinical intestinal calibre and demonstrated its ability in detecting both functional and structural information in various intestinal environments.

Declaration of Competing Interest

The authors declare that there are no conflicts of interest.

Acknowledgements

This work was supported by National Key Research and Development Program of China (2018YFC0116302); National Natural Science Foundation of China (61975226, 82027803); Scientific Instruments

Funding of Chinese Academy of Sciences (YJKYQ20190077); CAS Key Laboratory of Health Informatics (2011DP173015); Natural Science Foundation of Guangdong Province (2021A1515011949); Guangdong Provincial Key Laboratory of Biomedical Optical Imaging Technology (2020B121201010); Basic and Applied Basic Research Foundation of Guangdong Province (2019A1515110727); Shenzhen Engineering Laboratory for Diagnosis & Treatment key technologies of interventional surgical robots.

Appendix A. Supporting information

Supplementary data associated with this article can be found in the online version at doi:10.1016/j.pacs.2022.100441.

References

- [1] The global cancer observatory, World Health Organization. International Agency for Research on Cancer, 2020.
- [2] K.M. Schieffer, B.P. Kline, G.S. Yochum, W.A. Koltun, Pathophysiology of diverticular disease, *Expert Rev. Gastroenterol. Hepatol.* 12 (7) (2018) 683–692.
- [3] C. Fiocchi, Inflammatory bowel disease: etiology and pathogenesis, *Gastroenterology* 115 (1) (1998) 182–205.
- [4] T. Guo, X. Lu, A. Yang, W. Zhou, F. Yao, X. Wu, L. Wang, C. Lu, G. Fei, H. Shu, D. Wu, Y. Li, X. Li, J. Qian, Enhanced magnifying endoscopy for differential diagnosis of superficial gastric lesions identified with white-light endoscopy, *Gastric Cancer* 17 (2014) 122–129.
- [5] R. Singh, V. Owen, A. Shonde, P. Kaye, C. Hawkey, K. Ragnath, White light endoscopy, narrow band imaging and chromoendoscopy with magnification in diagnosing colorectal neoplasia, *World J. Gastrointest. Endosc.* 1 (1) (2009) 45–50.
- [6] Y. Suo, F. Wu, P. Xu, H. Shi, T. Wang, H. Liu, Z. Cheng, NIR-II fluorescence endoscopy for targeted imaging of colorectal cancer, *Adv. Healthc. Mater.* 8 (2019), 1900974.
- [7] Z. Liu, S. Miller, B. Joshi, T. Wang, In vivo targeting of colonic dysplasia on fluorescence endoscopy with near-infrared octapeptide, *Endoscopy* 62 (2013) 395–403.
- [8] T. Tsai, J. Fujimoto, H. Mashimo, Endoscopic optical coherence tomography for clinical gastroenterology, *Diagnostics* 4 (2) (2014) 57–93.
- [9] M. Gora, M. Suter, G. Tearney, X. Li, Endoscopic optical coherence tomography: technologies and clinical applications, *Biomed. Opt. Express* 8 (5) (2017) 2405–2444.
- [10] M. Byrne, P. Jowell, Gastrointestinal imaging: endoscopic ultrasound, *Gastroenterology* 122 (6) (2002) 1631–1648.
- [11] S. Kelly, K. Harris, E. Berry, J. Hutton, P. Roderick, J. Cullingworth, L. Gathercole, M. Smith, A systematic review of the staging performance of endoscopic ultrasound in gastro-oesophageal carcinoma, *Gut* 49 (4) (2001) 534–539.
- [12] J. Gonzalo-Marin, J. Vila, M. Perez-Miranda, Role of endoscopic ultrasound in the diagnosis of pancreatic cancer, *World J. Gastrointest. Oncol.* 6 (9) (2014) 360–368.
- [13] A. Attia, G. Balasundaram, M. Moothanchery, U. Dinish, R. Bi, V. Ntziachristos, M. Olivo, A review of clinical photoacoustic imaging: current and future trends, *Photoacoustics* 16 (2019), 100144.
- [14] J. Kim, D. Lee, U. Jung, C. Kim, Photoacoustic imaging platforms for multimodal imaging, *Gastroenterology* 34 (2) (2015) 88–97.
- [15] W. Choi, E. Park, S. Jeon, C. Kim, Clinical photoacoustic imaging platforms, *Biomed. Eng. Lett.* 8 (2018) 139–155.
- [16] C. Wang, F. Lu, M. Cai, Z. Xiang, G. Zheng, Stomach wall structure and vessels imaging by acoustic resolution photoacoustic microscopy, *World J. Gastroenterol.* 24 (31) (2018) 3531–3537.
- [17] H.Q. Wu, H.Y. Wang, W.M. Xie, S.L. Wu, Z.F. Li, X.M. Zhang, H. Li, Scanning photoacoustic imaging of submucosal gastric tumor based on a long focused transducer in phantom and in vitro experiments, *J. Innov. Opt. Health Sci.* 12 (03) (2019), 1950011.
- [18] J. Kim, J. Ahn, G. Kang, J.H. Hwang, C. Kim, High-resolution photoacoustic/ultrasound imaging of the porcine stomach wall: an ex vivo feasibility study, *Biomed. Opt. Express* 12 (11) (2021) 6717–6729.
- [19] J. Yang, C. Favazza, R. Chen, J. Yao, X. Cai, K. Maslov, Q. Zhou, K. Shung, L. Wang, Simultaneous functional photoacoustic and ultrasonic endoscopy of internal organs in vivo, *Nat. Med.* 18 (8) (2012) 1297–1303.
- [20] Y. Li, Z. Zhu, J. Jing, J. Chen, A. Heidari, Y. He, J. Zhu, T. Ma, M. Yu, Q. Zhou, Z. Chen, High-speed integrated endoscopic photoacoustic and ultrasound imaging system, *IEEE J. Sel. Top. Quantum Electron.* 25 (1) (2019), 7102005.
- [21] Y. Li, G. Lu, Q. Zhou, Z. Chen, Advances in endoscopic photoacoustic imaging, *Photonics* 8 (7) (2021) 281.
- [22] Y. Li, R. Lin, C. Liu, J. Chen, H. Liu, R. Zheng, X. Gong, L. Song, In vivo photoacoustic/ultrasonic dual-modality endoscopy with a miniaturized full field-of-view catheter, *J. Biophoton.* 11 (10) (2018), e201800034.
- [23] K. Xiong, S. Yang, X. Li, D. Xing, Autofocusing optical-resolution photoacoustic endoscopy, *Opt. Lett.* 43 (8) (2018) 1846–1849.
- [24] X. Leng, W. Chapman, B. Rao, S. Nandy, R. Chen, R. Rais, I. Gonzalez, Q. Zhou, D. Chatterjee, M. Mutch, Q. Zhu, Feasibility of co-registered ultrasound and acoustic-resolution photoacoustic imaging of human colorectal cancer, *Biomed. Opt. Express* 9 (11) (2018) 5159–5172.

- [25] Z. Ali, C. Zakian, Q. Li, J. Gloriod, S. Crozat, F. Bouvet, G. Pierre, V. Sarantos, M. Di Pietro, K. Flisikowski, P. Andersen, W. Drexler, V. Ntziachristos, 360°optoacoustic capsule endoscopy at 50 Hz for esophageal imaging, *Photoacoustics* 25 (2022), 100333.
- [26] Y. Yuan, S. Yang, D. Xing, Preclinical photoacoustic imaging endoscope based on acousto-optic coaxial system using ring transducer array, *Opt. Lett.* 35 (13) (2010) 2266–2268.
- [27] Q. Tan, C. Wang, J. Liu, J. Huang, Y. Li, Y. Xiao, G. Xia, T. Ma, H. Zheng, Ultrafast endoscopic ultrasonography with circular array, *IEEE Transactions on Medical Imaging* 39(6): 2110–2120.
- [28] G.-P. Lopes, M.-M. Ferreira-Silva, A.-A. Ramos, H. Moraes-Souza, A. Prata, D. Correia, Length and caliber of the rectosigmoid colon among patients with Chagas disease and controls from areas at different altitudes, *Rev. da Sociedade Bras. De. Med. Trop.* 46 (6) (2013) 746–751.
- [29] R. Boellaard, N.C. Krak, O.S. Hoekstra, A.A. Lammertsma, Effects of noise, image resolution, and ROI definition on the accuracy of standard uptake values: a simulation study, *J. Nucl. Med.* 45 (9) (2004) 1519–1527.
- [30] R. Berretta, T.S. Patrelli, C. Migliavacca, M. Rolla, L. Franchi, M. Monica, S. Gizzo, Assessment of tumor size as a useful marker for the surgical staging of endometrial cancer, *Oncol. Rep.* 31 (5) (2014) 2407–2412.



Riqiang Lin received his M.Sc. and B.S. degree from Shenzhen University. He is currently pursuing his Doctoral degree at The Hong Kong Polytechnic University and focuses on the research of photoacoustic endoscopy imaging and ultrasound transducer technology. He has developed a series of novel photoacoustic systems, including optical resolution and acoustic resolution photoacoustic microscopy, full field-of-view photoacoustic endoscopy.



Xi Tian Wang is a Ph.D candidate at Beijing Institute of Technology, received both his Master and Bachelor degree from Beijing Institute of Technology in 2017 and 2013. Now he is a visiting student of Shenzhen Institute of Technology, Chinese Academy of science, working on applying novel physical mechanisms for photoacoustic functional imaging.



Zhihua Xie is an Associate Professor at SIAT, CAS. She received her Ph.D. degree from the University of Franche-Comte, France, 2016. She joined SIAT in October, 2016. Dr. Xie's research focuses on the development and applications of photoacoustic endoscopies.



Jiamei Liu received her B.S. degree from Hainan normal University, China, in 2015, and her M.Sc. degree from Xiangtan University, China, in 2018. She was a visiting student with the Institute of Biomedical and Health Engineering in Shenzhen Institutes of Advanced Technology (SIAT), Chinese Academy of Sciences, Shenzhen, China, from 2016 to 2018. Currently she is a Research assistant of SIAT. Her research interest is in biomedical ultrafast ultrasound imaging.



Qingyuan Tan received the B.S. degree in mathematics and applied mathematics from Wuhan University, China, in 2017, and the M.Eng. degree from the State Key Laboratory of LIEMASRS, Wuhan University, in 2020. He was a Visiting Student with the Institute of Biomedical and Health Engineering, Shenzhen Institutes of Advanced Technology (SIAT), Chinese Academy of Sciences, Shenzhen, China, from 2018 to 2021. His research interest is in biomedical ultrafast ultrasound imaging.



Yaguang Ren is an Assistant Professor at SIAT, CAS. In 2018, she got the Ph.D. degree in bioengineering at the Hong Kong University of Science and Technology, Hong Kong, China. Her research interest includes the development of photoacoustic imaging, fluorescent microscope imaging and image processing.



Shengmiao Lv is currently pursuing his Master's degree in Shenzhen Institutes of Advanced Technology, Chinese Academy of Science. His research interests include photoacoustic endoscopy imaging and FPGA-based digital signal processing system



Jiqing Huang is an assistant engineer at SIAT, CAS. He received his bachelor's degree from Dongguan City University in 2015. He is mainly engaged in the research and development of ultrasonic transducers



Liang Song is a Professor at SIAT, CAS and founding directors of The Research Lab for Biomedical Optics, and the Shenzhen Key Lab for Molecular Imaging. Prior to joining SIAT, he studied at Washington University, St. Louis and received his Ph.D. in Biomedical Engineering. His research focuses on multiple novel photoacoustic imaging technology.



Chengbo Liu is a Professor at SIAT, CAS. He received both his Ph.D and Bachelor degree from Xi'an Jiaotong University, each in 2012 in Biophysics and 2007 in Biomedical Engineering. During his Ph.D. training, he spent two years doing tissue spectroscopy research at Duke University as a visiting scholar. Now he is working on multi-scale photoacoustic imaging and its translational research.



Teng Ma received the B.S.E. degree from the University of Michigan in 2011 and the M.S. and Ph.D. degrees in biomedical engineering from the University of Southern California in 2013 and 2015, respectively. He conducted his doctoral and post-doctoral research about advanced ultrasonic imaging technologies at the NIH Resource Center for Medical Ultrasonic Transducer Technology, University of Southern California. In 2017, he joined the Shenzhen Institute of Advanced Technology (SIAT), Chinese Academy of Sciences (CAS), Shenzhen, China, where he is currently a Professor with Paul C. Lauterbur Research Center for Biomedical Imaging. He conducts research primarily about biomedical ultrasound technology and multi-modality imaging techniques. He is also actively working in translational research and medical device commercialization with entrepreneurial spirit to translate innovative technology from research to clinical benefits.



Xiaojing Gong is a professor at SIAT, CAS. He received his B.S. degree in Mechatronics from the Southeast University in 2000, and Ph.D. degree in Fine Instruments and Mechanics from the University of Science and Technology of China in 2007. Since joined the IBHE of SIAT in 2007, Dr. Gong focuses on the development of the endoscopic systems based on optical and ultrasound principals (including photoacoustic imaging, OCT imaging, ultrasound imaging, etc). Meanwhile, Dr.Gong also put research emphasis on the application and clinical translation of the novel endoscopies, such as the intravascular imaging, intra-intestinal tract imaging, intra-uterus imaging, etc.